Assimilating Coastal Wave Observations in Regional Swell Predictions. Part I: Inverse Methods

W. C. O'REILLY AND R. T. GUZA

Center for Coastal Studies, Scripps Institution of Oceanography, La Jolla, California

(Manuscript received 12 September 1996, in final form 24 July 1997)

ABSTRACT

Inverse methods are used to assimilate wave observations into numerical predictions of ocean swell (0.04–0.12 Hz surface waves) propagating over complex continental shelf bathymetry. Model predictions of swell on the shelf can be degraded by the limited accuracy and resolution of the initializing offshore (unsheltered deep water) frequency–directional spectra S_o, usually derived from buoy measurements or meteorological hindcasts. The authors use a spectral refraction wave propagation model to find improved estimates of S_o that are consistent with both unsheltered and sheltered (altered by coastal bathymetry) observations, and vary smoothly in direction and time.

In Part I, linear and nonlinear inverse assimilation methods are developed. Their potential and limitations are illustrated qualitatively using a scenario where no a priori knowledge of S_o is used in the inverse estimates. Inverse estimates of S_o based solely on sheltered wave data routinely collected in the Southern California Bight are compared to meteorological hindcasts of peak offshore swell directions for two time periods dominated by swell arrivals from a distant storm. Robust model–hindcast agreement for the peak direction of an energetic, unimodal North Pacific swell event demonstrates that offshore directional information can be inferred solely from sheltered measurements. The poor model–hindcast agreement for a south swell event is markedly improved by the a priori assumption that S_o is unimodal with a prescribed parametric form, but assumptions about the shape of S_o severely reduce the generality of the approach. The authors conclude that conventional (low directional resolution) measurements from a few sheltered sites cannot be used to routinely resolve S_o, and offshore measurements or hindcasts of S_o are needed as additional constraints in practical applications.

In Part II, the inverse methods are generalized to include hindcasts or unsheltered directional buoy data as primary constraints and sheltered observations are used to enhance the directional resolution and stability of S_o. Initialized with these S_o, the wave model yields improved predictions of regional swell conditions. The value of assimilating coastal observations into regional wave predictions is demonstrated with a comprehensive field study.

1. Introduction

Two approaches are typically used to estimate swell (0.04–0.12 Hz surface waves generated by distant storms) at uninstrumented coastal locations: 1) by interpolating or extrapolating from nearby wave measurements or 2) by initializing a wave propagation model with offshore directional wave observations or meteorological-based hindcasts. In regions with complicated offshore and local bathymetry (e.g., Fig. 1), the first approach often fails because of the extreme spatial variability of the sheltered (altered by coastal bathymetry) wave field (Pawka 1983). The second approach is potentially more accurate, but high-resolution estimates of the offshore directional spectrum S_o are needed to properly initialize models for wave propagation over complex bathymetry. For example, coastal sites in the Southern California Bight (Fig. 1) are typically exposed to only a narrow range of incident North Pacific swell directions due to the blocking effects of the offshore islands. Sensitivity analyses (O'Reilly and Guza 1993) suggests that the resolution of directional wave spectra from global wave generation models (e.g., The WAMDI Group 1988) and from directional buoys (Ochoa and Gonzalez 1990) may be insufficient to initialize wave models applied to bathymetrically complex coastal regions such as southern California.

We assume that the limited accuracy and resolution of the offshore directional spectra S_o is a significant source of error in regional swell predictions. Improved estimates of S_o (and hence of the modeled regional wave field) are obtained by using inverse methods to assimilate sheltered wave observations into a linear wave propagation model. The basic methodology is developed in Part I. The potential and limitations of the approach are illustrated using a scenario where no a priori knowl-

Corresponding author address: Dr. William C. O'Reilly, University of California, San Diego, Scripps Institution of Oceanography, Center for Coastal Studies, 0209, 9500 Gilman Drive, La Jolla, CA 92093-0209.
E-mail: woreilly@ucsd.edu

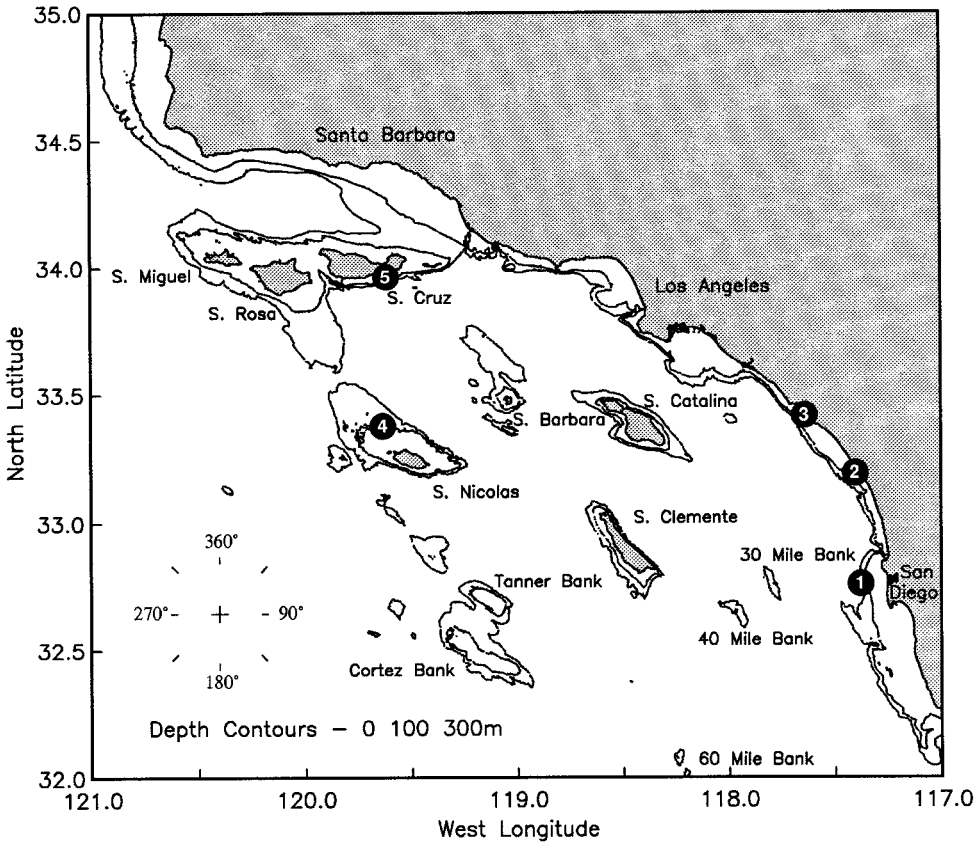

FIG. 1. The Southern California Bight. Numbered circles are selected Coastal Data Information Program measurement stations used in inverse estimates (see section 2).

edge of S_o is used in the inverse estimates. Inverse estimates of S_o based solely on sheltered wave data routinely collected in the Southern California Bight are qualitatively compared to meteorological hindcasts of peak offshore swell directions for two time periods dominated by swell arrivals from a distant storm. In Part II, the inverse model is generalized to include hindcasts and unsheltered buoy data as observations and additional coastal wave measurement stations are used to validate the resulting inverse-based regional swell predictions.

Linear spectral refraction theory (Pierson et al. 1953; Longuet-Higgins 1957) is used to model the transformation of offshore frequency–directional wave spectra over complex coastal bathymetry. The theory, extended to include estimates of wave energy propagation time lags between offshore waters and coastal sites, defines the time-dependent relationship between wave observations at sheltered sites and the evolving offshore frequency–directional swell spectra, $S_o(f, \theta_o, t)$, where f is frequency, θ_o is the offshore propagation direction, and t is time. Wave generation (by wind) and dissipation (by breaking and other processes) are neglected. These and other assumptions presently restrict the method to areas with dimensions less than several hundred kilometers, and to situations with no significant regional wind wave generation (e.g., to swell frequencies, or to time periods when regional winds are low). Standard inverse methods result in S_o that are (statistically) consistent with the nondirectional and low directional resolution (e.g., directional buoy) sheltered measurements. There are, however, many consistent S_o. Smoothness constraints are commonly used to ensure unique solutions in geophysical inverse problems (e.g., Provost and Salmon 1986). In the first inverse approach, we impose smoothness on S_o over direction at a fixed frequency (e.g., Long and Hasselmann 1979) and also over time for individual frequency–directional components. The second, nonlinear inverse approach includes the same temporal smoothness constraint but the stronger directional constraint that S_o has a unimodal, cosine–power law directional distribution (Longuet-Higgins et al. 1963).

Coastal wave observations are described in section 2. In section 3, the linear spectral refraction wave model is used to express the relationship between S_o and the coastal observations as a set of linear equations. Smoothness constraints in direction and time, and weighting of observations by their statistical uncertainty, are added to the inverse problem is section 4. In

section 5, inversely estimated directional distributions are compared to meteorological hindcast estimates of the peak offshore swell direction, for two wave fields believed to be dominated by a single distant source. Robust agreement for the peak directions of an energetic, unimodal North Pacfic swell event shows that offshore directional information can be inversely inferred from sheltered measurements using linear wave theory. However, other estimated characteristics of S_o are sensitive to the somewhat arbitrary values selected for the smoothness weights, and inverse–hindcast agreement for the peak direction of a South Pacific swell event is marginal, demonstrating the limitations of the method when only a few sheltered observation sites are available. In section 6, S_o estimates based on the a priori assumption of a unimodal cosine–power law directional distribution are shown to be consistent with the hindcast directions and expected narrow directional distributions for both swell events. The additional information (that a unimodal distribution is expected) enhances the inverse solutions derived from these small datasets. However, unimodality is too severe a constraint for general application. The results are summarized in section 7.

2. Coastal wave observations

Long-term ocean wave measurements are typically made with pressure sensors and surface buoys. Nondirectional buoys and single pressure sensors yield estimates of wave energy,

$$\int_0^{2\pi} d\theta\, S(f, \theta), \tag{2.1}$$

where $S(f, \theta)$ is the frequency–directional spectral density. Directional (pitch–roll or translational) buoys directly estimate (i.e., without assumptions about the shape of S) four directional moments, corresponding to linear combinations of cross-spectra between the measured sea surface elevation and the two components of sea surface slope (Longuet-Higgins et al. 1963),

$$\int_0^{2\pi} d\theta\, S(f, \theta) \cos\theta$$

$$\int_0^{2\pi} d\theta\, S(f, \theta) \sin\theta$$

$$\int_0^{2\pi} d\theta\, S(f, \theta) \cos 2\theta$$

$$\int_0^{2\pi} d\theta\, S(f, \theta) \sin 2\theta. \tag{2.2}$$

Slope arrays (four pressure sensors in a square configuration with small physical dimensions compared to a wavelength) measure these same directional moments (Higgins et al. 1981; Herbers and Guza 1989). The directional resolution of slope arrays and buoys is inherently limited because the measured quantities, (2.1) and (2.2), are only the first few terms in a Fourier expansion of $S(f, \theta)$ (Longuet-Higgins et al. 1963; Ochoa and Gonzalez 1990). However, even low-resolution directional data at sheltered sites provide useful additional constraints on the shape of S_o.

The inverse methodologies are applied to observations from the Southern California Bight (Fig. 1) collected in 1984–85 by the Coastal Data Information Program (Seymour et al. 1985; 1994). Nondirectional buoy measurements were made at heavily sheltered sites 1 (200-m depth, Fig. 1) and 5 (70-m depth) (Fig. 1) and at a more exposed but still sheltered location near San Nicolas Island (site 4, 100-m depth). Slope arrays were deployed at 10-m depth at heavily sheltered sites 2 and 3. Data records, of 17-min duration with a 1-Hz sample rate, were collected at intervals of either 3 or 6 hours.

3. The forward model

a. Linear spectral refraction

Measured variations in sheltered swell wave energy (2.1) and directional moments (2.2) are used to estimate inversely the unsheltered, deep water swell directional spectra S_o from which the sheltered waves originated. Central to the inverse methodology is a ''forward'' model defining the relationship between S_o and coastal observations. Linear, spectral refraction theory (Pierson et al. 1953; Longuet-Higgins 1957) transforms continuous offshore directional spectra $S(f, \theta_o)$ of arbitrary shape to sheltered spectra, $S(f, \theta)$,

$$S(f, \theta) = \frac{k}{k_o}\frac{C_{go}}{C_g} S_o[f, \Gamma(f, \theta)], \tag{3a.1}$$

where k is the wavenumber magnitude (related to the frequency f and water depth through the linear dispersion relation), C_g is the group velocity, the subscript o denotes offshore, and unsubscripted variables are at sheltered sites. The frequency-dependent relationship $\theta_o = \Gamma(f, \theta)$ between offshore wave angles θ_o and sheltered wave angles θ is obtained by backward ray tracing from a single sheltered location into unsheltered deep water (Fig. 2), where it is assumed that S_o is spatially homogeneous (an assumption further restricting the present study to swell generated by distant storms). Examples of sheltering in the Southern California Bight [based on (3a.1)] are given in O'Reilly and Guza (1993).

The caustics that plague traditional nonspectral ray methods do not occur in the spectral approach and finite amplitude waves are predicted at locations where forward propagating rays would cross (Dorrestein 1960; LeMehaute and Wang 1982; Graber et al. 1990, 1991). Comparisons to more complete models that include both refraction and diffraction show that spectral refraction models overestimate maximum wave heights

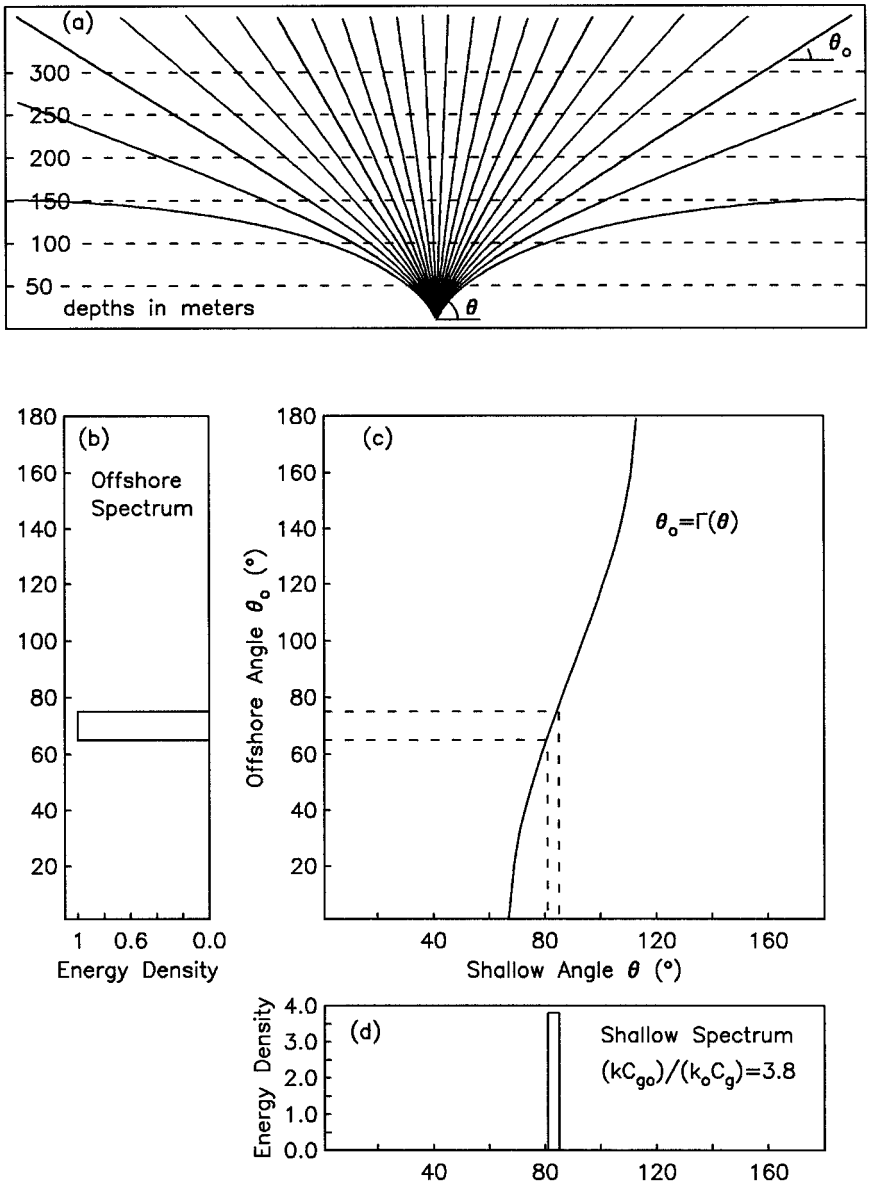

FIG. 2. The refractive transformation (3a.1) of an offshore directional spectrum of 0.06-Hz frequency waves propagating over planar bathymetry into 10-m depth; 90° is normally incident to the coast. Backward ray tracing (a) is used to define the angle transformation function, Γ, (c). A 10°-wide rectangular offshore directional spectrum with unity energy density (b) is mapped to a narrower (~5°) shallow water spectrum by refraction using Γ (b to c to d). The energy density is amplified by a factor of 3.8 (d) due to both shoaling and refraction. k = wavenumber, C_g = group velocity, and the subscript o denotes offshore deep water.

in the lee of shoals when the incident spectrum S_o is extremely narrow in both frequency and direction (O'Reilly and Guza 1991). However, when S_o is relatively broad or the sheltered site is in the far-field of complex bathymetric features, diffraction effects are weaker. O'Reilly and Guza (1993) discuss the relative merits of models with and without diffraction in regional wave modeling. Diffraction is neglected in the forward model used here (3a.1) and the selected coastal observations (Fig. 1) are from areas with relatively mild (and well surveyed) local bathymetry.

Given S_o, the spectral refraction model (3a.1) provides estimates of the continuous sheltered wave spectrum S. However, the field measurements yield only directionally integrated properties of S (2.2). Therefore, (3a.1) is combined with (2.1) and (2.2) to produce a forward model that predicts the measured integral properties of the wave field at a fixed wave frequency,

$$\int_0^{2\pi} S(f, \theta) m_p(\theta)\, d\theta = \frac{k}{k_o}\frac{C_{go}}{C_g}\int_0^{2\pi} S_o[f, \Gamma(f, \theta)] m_p(\theta)\, d\theta;$$

$$p = 1, 2, 3, 4, 5, \qquad (3a.2)$$

where $m_1(\theta) = 1$, $m_2(\theta) = \cos\theta$, $m_3(\theta) = \sin\theta$, $m_3(\theta) = \cos 2\theta$, and $m_4(\theta) = \sin 2\theta$.

Remotely generated swell observed at sheltered southern California sites agrees well with spectral refraction predictions initialized with data from an offshore directional buoy (O'Reilly et al. 1994 and Part II). These results suggest that the present, relatively simple, forward model incorporates the swell propagation processes dominant in southern California: shoaling and refraction over variable depths, ''blocking'' or ''shadowing'' of sites in the lee of islands, and propagation time lags (see below). The inverse approach can be used with the more sophisticated propagation models undoubtedly needed for other regions where processes neglected in the present forward model (e.g., diffraction, wave–current interaction, wave generation and dissipation, and nonlinear interactions) are important.

b. The discrete forward model

To simplify the inverse problem, the continuous unsheltered swell spectrum $S_o(f, \theta_o)$ in (3a.2) is discretized into frequency–directional components with finite directional and frequency bandwidth and constant energy density within a given component. The frequency bandwidth of 0.01 Hz selected for both discrete forward modeling and analysis of the wave measurements (described in section 2) is a compromise between maximizing resolution (with a narrow bandwidth) and minimizing forward modeling errors and data statistical uncertainty (by averaging over a broad bandwidth). The transformation of each discrete band is numerically simulated by averaging spectral refraction results for 11 subfrequencies uniformly distributed across the bandwidth.

There is no exchange of energy between frequencies in this linear model, so each 0.01-Hz band is treated as a separate forward or inverse problem, and the frequency dependence is often omitted in the notation below. In each frequency band, S_o is discretized into a vector of N 5° directional bins

$$\mathbf{S}_o = [S_{o1}, S_{o2}, S_{o3}, \cdots, S_{oN}]^{\mathrm{T}}, \qquad (3b.1)$$

where T is the transpose. In southern California, the range of possible incident offshore swell directions spans 180°, so $N = 36$. The 5° directional bandwidth of the discrete model was selected based on simulations by O'Reilly and Guza (1993) and represents a compromise between maximizing forward model accuracy with a narrow bandwidth and minimizing the number of unknowns in the resulting inverse problem (discussed in section 4) with fewer, broad directional bands.

The wave observations are analyzed using the same 0.01-Hz resolution and combined to form (at each frequency) a data vector **b**:

$$\mathbf{b} = [b_1, b_2, b_3, \cdots, b_M]^{\mathrm{T}} \qquad (3b.2)$$

with each component representing a measurement of energy or one of the four directional moments (2.2). The total number of observations M varies depending on the number of coastal measurement stations and whether or not they are directional.

To construct the discrete forward wave model, each component of the offshore directional distribution $\mathbf{S}_o$ is assigned unit energy density and substituted into (3a.2) to obtain the linear transfer coefficients $\mathbf{A}$ between offshore and the sheltered coastal observations **b**. The theoretical relationship between the offshore directional spectrum and sheltered measurements is thus approximated as a set of linear equations

$$b_i = \sum_{j=1}^{N} A_{ij} S_{oj}, \qquad (3b.3)$$

where S_{oj} is the jth offshore directional component, b_i is the ith coastal observation (of energy or a directional moment), and A_{ij} are elements of the linear-theory-based data kernel matrix.

c. A time-dependent forward model for nonstationary swell

Spectral transformations based on (3a.2) neglect the transit time for wave energy propagating between measurement sites. As swell from distant sources arrive and recede in southern California, nonstationarity in wave energy in frequency bands 0.01 Hz wide (the selected resolution of the forward model) occurs over 3–4 h (Elgar and Seymour 1985), whereas typical energy propagation times across the entire region are 7 h for 20-s period waves and 22 h for 8-s waves. The energy (in a particular frequency band) from a distant storm can be simultaneously increasing at one site and waning at a different site closer to the storm location. In fact, time lags between energy arrivals at different observation sites provide additional information about the wave propagation direction. The forward model is extended to include frequency and direction dependent time lags, $\tau(f, \theta)$, estimated using group-velocity-based propagation times along the ray trajectories between each observation site and unsheltered deep water. The ray paths terminate offshore at different locations, and simple geometry is used to adjust the lag times relative to a single arbitrary offshore site. Propagation related time lags are thus accounted for both offshore and within the bight. Although S_o is spatially homogeneous offshore, the time lags create slightly

different time variations of S_o at different offshore sites. Results for S_o shown below are for an unsheltered deep water site in approximately the center of the bight (Fig. 1). Adding time lags to (3a.2) yields

$$\int_0^{2\pi} S(f,\ \theta,\ t)m_p(\theta)\ d\theta = \frac{k}{k_o}\frac{C_{go}}{C_g}\int_0^{2\pi} S_o[f,\ \Gamma(f,\ \theta),\ t+\tau(f,\ \theta)]m_p(\theta)\ d\theta;$$
$$p = 1,\ 2,\ 3,\ 4,\ 5. \qquad (3c.1)$$

To obtain a discrete, time-dependent equivalent of (3c. 1), the average τ in each 5° direction bin of $\mathbf{S}_o$ is rounded to the nearest hour. For each frequency band, the observation b_i is now the sum of contributions from the direction bins of the discrete offshore spectrum $\mathbf{S}_o$ over a range of hour time bins. Here τ is a function of the wave frequency and direction and of the relative locations of the arbitrary offshore site and each observation site. Time-dependent, hourly estimates of S_o are sought using observations spanning an M hour time period. A single observation, made up of contributions from the N direction bins of $\mathbf{S}_o$ with a range of different time lags, can be expressed as a linear combination of NM direction–time bins,

$$b_i = \sum_{j=1}^{NM} A_{ij}S_{oj}. \qquad (3c.2)$$

Relative to the time-independent model (3b.4), the dimension j is increased by a factor of M in the more cumbersome time-dependent problem. In addition, the transformation matrix $\mathbf{A}$ becomes sparse as M increases because only N of the NM transformation coefficients in a row of $\mathbf{A}$ are nonzero. That is, each 5°-wide direction bin of $\mathbf{S}_o$ contributes only once, at a particular time lag τ, to the wave field at a specific sheltered site at a particular time t.

4. The linear inverse problem

a. Nonnegative least squares

The discretized, linear forward model (3c.2), rewritten in matrix notation as

$$\mathbf{b} = \mathbf{A}\mathbf{S}_o \qquad (4a.1)$$

can be solved by various techniques. We used nonnegative least squares (NNLS: Lawson and Hansen 1974) to find the nonnegative solution for S_o, in each 0.01-Hz frequency band, that is most consistent with $\mathbf{b}$ in a least squares (2-norm) sense

$$\min_{S_o \geq 0} \|\mathbf{A}\mathbf{S}_o - \mathbf{b}\|_2. \qquad (4a.2)$$

b. Directional and temporal smoothness constraints

In practice, the number of unknowns in the inverse problem (the directional components of S_o) greatly outnumber the knowns (observations), and the inverse problem is severely underdetermined. Reducing the number of unknowns by using fewer but wider direction bins is problematic because many sheltered sites are sensitive to small changes in deep ocean wave direction. O'Reilly and Guza (1993) and O'Reilly et al. (1994) show that coarser directional resolution can significantly degrade forward model results in the Southern California Bight. We ensure uniqueness by including smoothness constraints, as is common in geophysical inverse problems (e.g., Provost and Salmon 1986; Constable et al. 1987; and many others). The rationalization for smoothness constraints is that, away from the immediate generation area, S_o that fluctuate wildly in direction (Long and Hasselmann 1979) or time are physically implausible.

A simple, smooth $\mathbf{S}_o$ consistent with the sheltered observations is found by including penalties in the overall least square fit for directional and temporal roughness (energy differences in neighboring directional bins in the same hour, and differences in the same directional bin in neighboring hours, respectively). The smoothness constraints are implemented as additional rows in $\mathbf{A}$ with the general form,

$$\begin{matrix} w_d & -w_d & 0 & 0 & \\ 0 & w_d & -w_d & 0 & \\ 0 & 0 & w_d & -w_d & \\ & & 0 & w_d & \\ & & & 0 & \\ & & & & \ddots, \end{matrix} \qquad (4b.1)$$

where w_d is the directional smoothness weighting factor. The corresponding values of the column vector $\mathbf{b}$ (4a.1) are set equal to zero. With N direction and M time bins, there are $(N-1)M$ additional equations in $\mathbf{A}$ forcing smoothness between neighboring directional components in the same hour. The magnitude of w_d determines the penalty for directional roughness relative to temporal roughness and misfits with the wave observations. Similarly, $(M-1)N$ additional equations for temporal smoothness are included, and weighting factors of w_t and $-w_t$ are assigned to the columns of $\mathbf{A}$ corresponding to neighboring time bins for the same direction. Ideally, smoothness constraints eliminate the spurious, wildly varying solutions that result with no smoothing, but do not produce significant wave observation misfit or suppress plausibly narrow directional distributions and/or rapidly evolving frequency spectra. The selection of appropriate values of w_d and w_t is explored using field observations in section 5.

c. Observation uncertainty

The wave observations (section 2) contain both instrumental and statistical errors. For the relatively short

(typically 17 min) data records used here, instrumental errors are safely assumed to be much smaller than the statistical uncertainty. Following the standard methodology, each observation is weighted inversely by its statistical uncertainty. The observations **b** and the corresponding row of **A** are normalized by the square root of the estimated variances σ^2. For example, for the ith observation, b_i,

$$\frac{b_i}{\sigma_i} = \sum_{j=1}^{NM} \frac{A_{ij}}{\sigma_i} S_{oj}. \qquad (4c.1)$$

Statistical fluctuations are treated as independent even though directional moment estimates from a single buoy or slope array are correlated (Borgman et al. 1982). The additional complexity of including covariance effects in the measurement statistics is considered unwarranted until more significant sources of error (most notably in the forward model, O'Reilly and Guza, 1993) can be better quantified. Formula for estimating σ^2 are given in the appendix.

5. A qualitative comparison of inverse estimates and wave hindcasts

To demonstrate the potential and limitations of the inverse approach, estimates of $\mathbf{S}_o$ based solely on sheltered wave data, the spectral refraction model and smoothness constraints are qualitatively compared to meteorological-based hindcasts of both Northern and Southern Hemisphere swell performed by Pacific Weather Analysis (U.S. Army Corps of Engineers 1988; N. E. Graham 1991, personal communication). We selected two swell events during time periods when meteorological charts and observations (not included in this study) indicate swell off California was dominated by energetic arrivals from a single distant storm. The hindcast is for an offshore deep water site near the center of the bight for a time approximately corresponding to the maximum observed energy. Inverse estimates are compared only to the hindcast peak direction at the peak frequency because the peak direction of a swell from a distant source varies slowly over time (e.g., Munk et al. 1963) and can be accurately estimated using the group velocity of the peak period and the corresponding great circle path from Southern California to the center of the distant fetch. Hindcasts of the peak swell direction are relatively straightforward and their accuracy is considered to be independent of the details of the particular hindcast model used.

The coastal observations are used to inversely estimate S_o without any knowledge of the deep water hindcast. It is assumed that an unknown deep ocean wave spectrum S_o, spatially homogeneous outside the islands, propagates through the islands to the coastal sites with the transformation given by the time-dependent forward model. The temporal variation of S_o is determined inversely using only the sheltered observations, the forward model, and smoothness constraints. In the following examples, inverse solutions are sought for an $M = 36$ h time period. Offshore swell are constrained by the North American coastline to approach southern California from directions 155°–335° (Fig. 1), so there are $N = 36$, 5°-wide directional bins. Therefore, $\mathbf{S}_o$ has $NM = 1296$ direction–time bins (unknowns). Observations b originating from $\mathbf{S}_o$ entirely within the 36-h time period are used to constrain the solution (i.e., a measurement is only useful if all contributions from S_o are within the 36-h time window). For the selected case studies, up to five wave gauge stations are used, two of these being directional [five observations each, (2.1) and (2.2)] and the remainder nondirectional [one observation, (2.1)]. Several measurements from each station (polled every 3–6 h) are entirely the result of $\mathbf{S}_o$ within the 36-h time period. There are typically 50–60 observations (knowns) to constrain the solution of $\mathbf{S}_o$ (1296 unknowns) and the discrete inverse problem (4a.2) is underdetermined. Smoothness and data uncertainty constraints are applied as described in sections 4b and 4c.

a. 17 January 1985

Northern Hemisphere winter storms typically form in the northwest Pacific and travel eastward toward the Gulf of Alaska. A powerful storm in January 1985 instead moved south toward the Hawaiian Islands and generated waves approaching southern California from the west. Inverse estimates of hourly S_o over a 36-h period (1296 direction–time bins) were made using five measurement stations (Fig. 1, sites 1–5) that were polled every 6 h and provided a total of 54 observations of wave energies and directional moments. The temporal evolutions of inverse-estimated deep ocean directional spectra for the frequency band 0.055–0.065 Hz (containing the hindcast peak period of 17 s) are shown in Fig. 3 for fixed temporal smoothness $w_t = 0.001$ and four different values of directional smoothness w_d. In each case the directional maxima of the inverse solutions are approximately constant in time and consistent with the PWA meteorological hindcast peak direction (267°) at the height of the wave event. However, as w_d (the penalty for rapid variation over direction) increases, the directional estimates become increasingly broad (Fig. 3), and the estimated total (directionally integrated) offshore energy in this frequency band grows substantially and begins to fluctuate wildly in time (Fig. 4). Deviations from the solid line in Fig. 5 indicate the data misfit between the measured energies (**b**) and those predicted by applying the forward wave transformation model (**A**) to the inverse solution $\mathbf{S}_o$ (which is the best least squares fit to *both* the observation and smoothness constraints). Figure 5 shows that all four inverse solutions represented by Figs. 3 and 4 closely fit the observed wave energy (directional moments from sites 1 and 2, not shown,

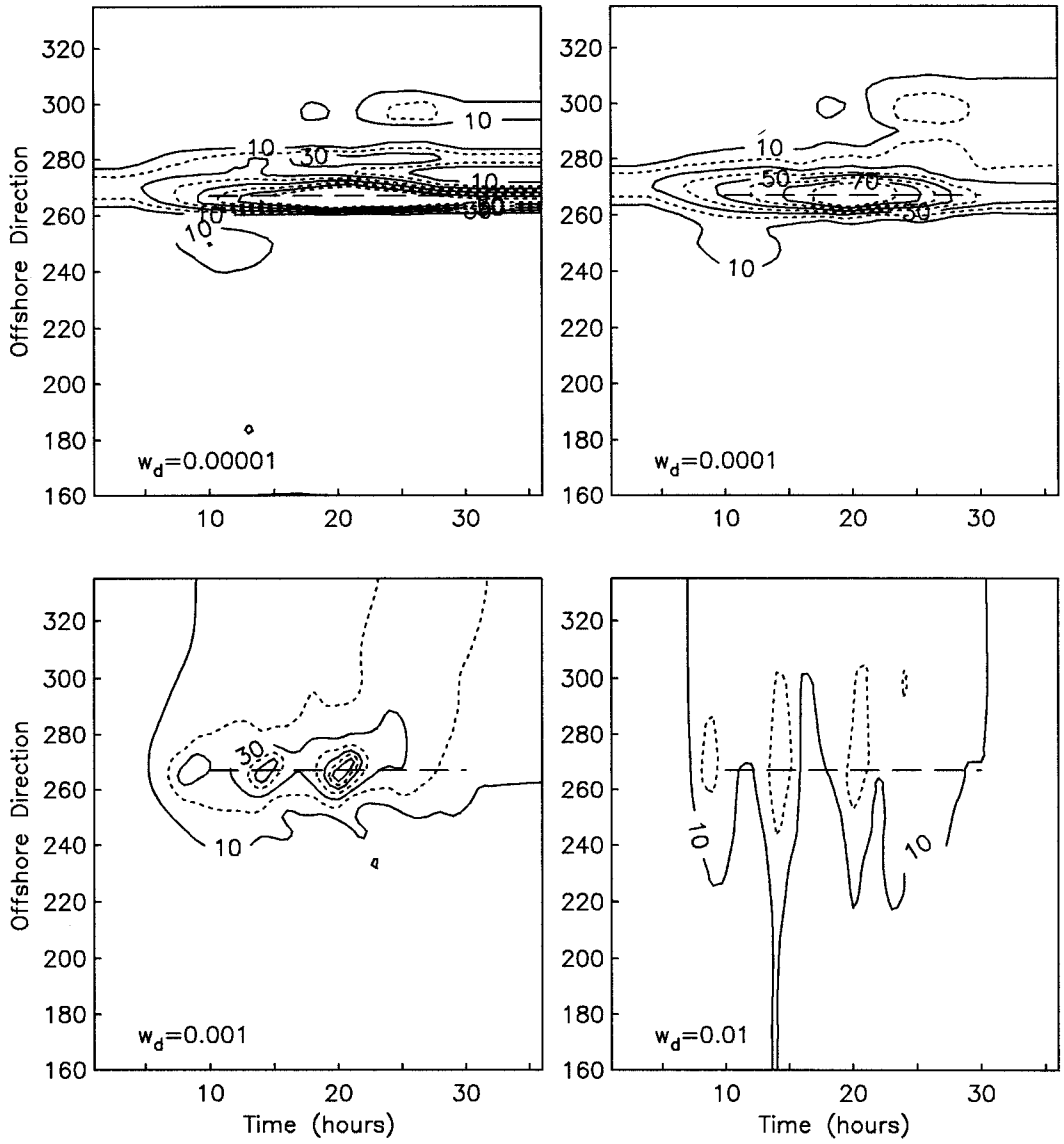

FIG. 3. Inverse estimates of offshore directional spectra (contour levels are in cm^2 deg^{-1}) for the frequency band 0.055–0.065 Hz for a 36-h period starting 0000 LST 17 January 1985. The four panels have the indicated directional smoothness weights w_d and temporal smoothness weight $w_t = 0.001$. The dashed line indicates the hindcast peak direction of 267° for ±10 h around the time of peak wave energy. Hindcast and inverse estimates are for unsheltered, deep water sites located near the center of the bight (Fig. 1).

were also closely fit). For all smoothness weights, the misfit is smaller than the statistical uncertainty of the data (the dashed lines are the 95% statistical confidence limits on the observations). The misfit is similarly small for fixed directional weight ($w_d = 0.0001$) and a range of temporal weights from 0.000 01 to 0.01 (not shown).

The inverse-estimated peak direction is considered reliable because it is insensitive to the choice of a wide range of directional (Fig. 3) and temporal (not shown) smoothness weights. However, other directional properties (e.g., directional width, Fig. 3), and the total energy contained within the frequency band (Fig. 4) vary dramatically with different weights. Figures 3–5 show that a wide range of smooth $\mathbf{S}_o$ satisfy the available observations, with the peak direction as the only common feature. The instrumented sites in this case are all significantly sheltered from north-northwest swells and are thus relatively insensitive to offshore energy arriving from these directions. The energy in $\mathbf{S}_o$ from north-northwest directions (e.g., 310°–330°) in the inverse estimates is therefore poorly constrained by the observations and depends largely on the relative size of the directional and temporal smoothness weights. An additional similarly sheltered observation site leads only to marginal improvement in constrain-

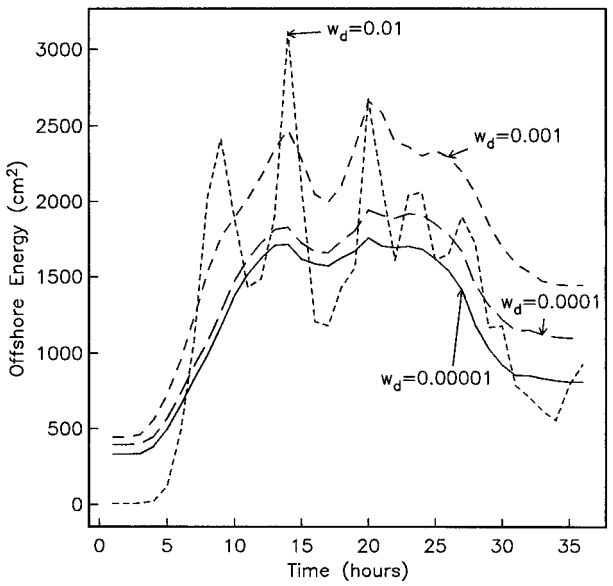

FIG. 4. Inverse estimates of offshore wave energy in the frequency band 0.055–0.065 Hz, starting 0000 LST 17 January 1985. The smoothness weight $w_t = 0.0001$ and the corresponding directional estimates (Fig. 3) are identified by their directional smoothness weights w_d.

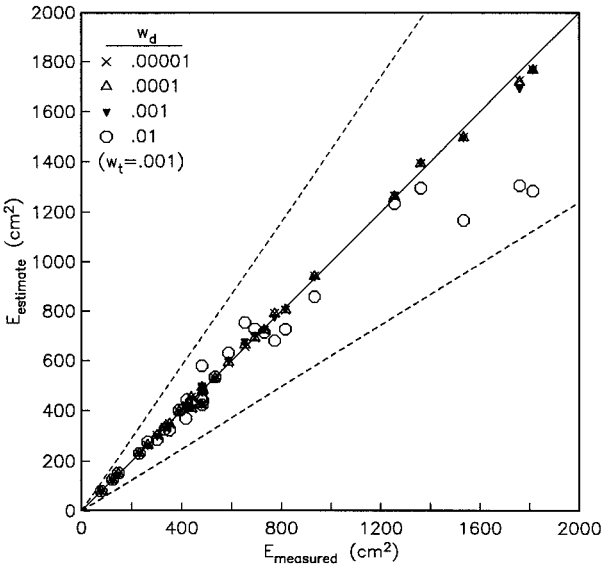

FIG. 5. Observation misfit of inverse-estimated energy for a range of different directional smoothness weights. The dashed lines represent the 95% confidence limits for the measurements and the solid line is zero misfit.

ing the offshore directional spectra for all possible incident directions. However, the wide variation in offshore energy predicted using only sheltered observations (Fig. 4) suggests that unsheltered wave energy measurements would greatly enhance inverse model performance. This is indeed the case, as shown in Part II.

b. 23 August 1984

A second linear inverse estimate is shown in Fig. 6 for an August 1984 Southern Hemisphere swell. The PWA hindcast peak period (at the time of maximum offshore power) was again 17 s (0.058 Hz), but with a peak direction of 198°. Four measurement stations (sites 2–5, Fig. 1) were used to form the inverse estimate. However, there were more total observations in this case (64) than the five-station January event because sites 1, 4, and 5 were polled more frequently (every 3 h). The inverse-estimated peak direction is within the proper southern quadrant (Fig. 6) but a single peak direction is not resolved, and the directional spread of energy is too broad for swell originating from the Southern Hemisphere (Munk et al. 1963). Figure 6 is typical of $\mathbf{S}_o$ estimated for a range of w_d and w_t.

A possible explanation for the poorer inverse model performance is that the coastal observation stations have similar exposure to waves from the south and cannot resolve narrow directional swell in this quadrant. The model resolution matrix (res $\mathbf{S}_o$) describes how well each 5° directional component of $\mathbf{S}_o$ can be resolved by a particular set of sheltered observations; res $\mathbf{S}_o$ for the complete linear inverse problem (4c.1) is not readily interpreted. Instead, we focus on the basic sheltering characteristics at the observation sites by using the initial, idealized inverse problem (3b.2) that excludes time lags, smoothness constraints, and data uncertainty. The N by N resolution matrix is calculated from $\mathbf{A}$ (3b.2) and is based on the generalized inverse for the underdetermined minimum length solution (Menke 1984),

$$(\text{res}\mathbf{S}_o) = \mathbf{A}^{\mathrm{T}}[\mathbf{A}\mathbf{A}^{\mathrm{T}}]^{-1}\mathbf{A}, \qquad (5b.1)$$

where the superscript T is the transpose and N is the number of directional bins of $\mathbf{S}_o$ (here $N = 36$). Values approaching unity along the main diagonal (of res $\mathbf{S}_o$) indicate deep ocean directions that are well resolved by the sheltered observation sites. The diagonal values are shown in Fig. 7 for the five observation sites in January 1985 and the four sites in August 1984. The larger values for the west swell peak direction ($\theta = 267°$) compared to the south peak direction indicate that the particular observation sites used here are, in theory, slightly better suited for resolving west swell, consistent with the better inverse performance for the January 1985 event. The severe sheltering of all the observation sites from northwest swell is apparent in the near-zero values for those directions (>310°, Fig. 7). The variability and overall low values of the resolution-matrix main diagonal indicate that the wave measurements are too spatially sparse and nonoptimally located to be used routinely with simple linear inverse methods.

Significant forward modeling errors may occur with south swell because the expected extremely narrow

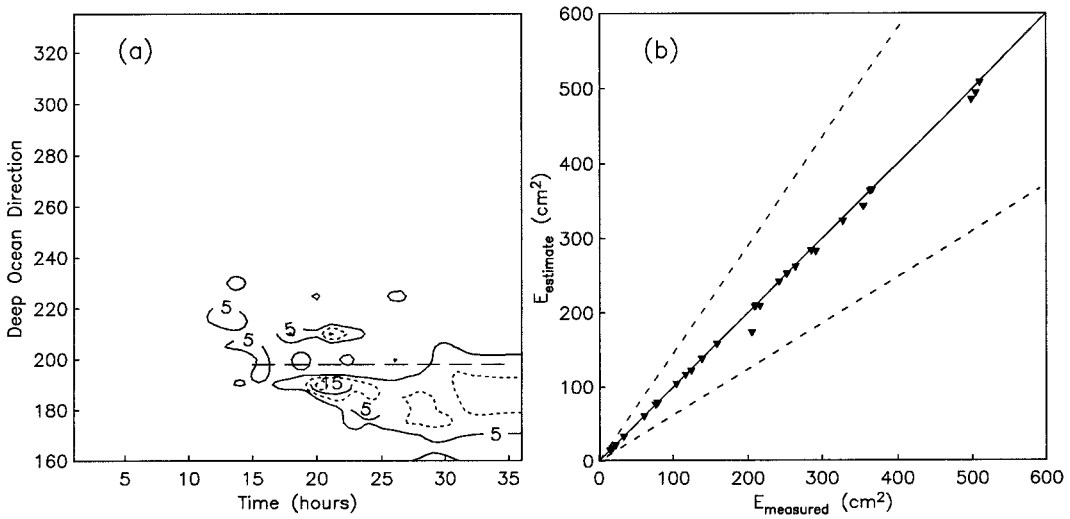

FIG. 6. (a) Contoured inverse estimates of deep water directional spectra (cm^2 deg^{-1}) and (b) observation misfit of energy, for the frequency band 0.055–0.065 Hz starting at 1200 LST 22 August 1984. Directional and temporal smoothness weights are $w_d = 0.0001$ and $w_t = 0.001$. The dashed line in (a) indicates the hindcast peak direction of 198 deg for ±10 h around the time of peak wave energy.

directional distributions increase the importance of diffraction (neglected here, see section 3) and of errors associated with the 5° bandwidth of the inverse estimates. However, in the next section we develop a nonlinear inverse method where S_o is assumed unimodal. The improved agreement with the hindcast suggests that the general linear inverse approach failed to resolve this swell event owing to the limited number and locations of the observation sites, rather than because of inaccuracies in the discretized forward model.

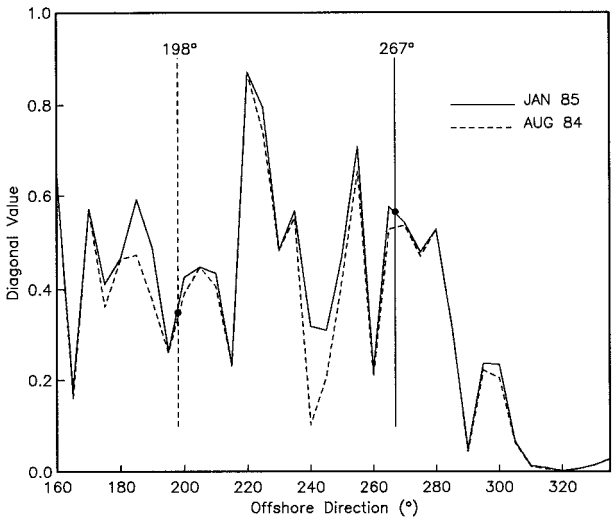

FIG. 7. Main diagonal values of the resolution matrix for $\mathbf{S}_o$ (5b.1) versus offshore wave direction, for the simplified linear inverse problem (3b.2). Vertical lines mark the peak directions of the meteorological hindcasts for the two historical swell events.

6. A priori directional forms: A nonlinear inverse problem

The many unknowns of the linear inverse problem are poorly constrained by the relatively small number of observations typically available so that simple smoothness constraints have an undesirably strong effect on the estimated S_o. Therefore, we consider an alternative approach analogous to one of the original methods used to inversely estimate directional spectra from the motion of a pitch–roll buoy (Longuet-Higgins et al. 1963). It is assumed a priori that the offshore wave field is dominated by waves from a single distant source and the deep ocean spectra (in each 0.01-Hz-wide frequency band) are prescribed to have a unimodal directional shape with the parametric form

$$S_o(\theta_o, t) = E_o(t)G \cos^{2s}[(\theta_p - \theta_o)/2], \quad (6.1)$$

where $E_o(t)$ is a temporally varying total (directionally integrated) energy density, θ_p is a fixed peak offshore wave direction, θ_o is the offshore direction, and G is a normalization constant that depends on s, the directional spreading parameter.

For simplicity, best-fit solutions are found by mapping the solutions over all plausible θ_p and s values and selecting the best overall fit, rather than by employing an iterative search. The nonlinear relationship between the coastal observations and the directional parameters θ_p and s (6.1) is solved for fixed values of θ_p and s (i.e., fixed directional shapes) with the spectral refraction model to define a linear relationship between the discrete time series of hourly offshore wave energy, $\mathbf{E}_o$, and the coastal observations, $\mathbf{b}$:

TABLE 1. Nonlinear inverse model estimates of offshore peak swell direction θ_p and directional spread (full width at half-maximum power in degrees, FWHM) based on the a priori assumption that the spectrum has a $\cos^{2s}$ parametric shape, and using smoothness weight $w_t = 0.0005$.

Swell event	Frequency (Hz)	θ_p (°)	FWHM (°)	θ_p Hindcast (°)
Aug 1984	.055–.065	200	10	198
Jan 1985	.055–.065	265	15	267

$$b_i = \sum_{j=1}^{M} A_i^f E_{oj}, \tag{6.2}$$

where M is the number of hourly time bins and

$$A_i^f = \sum_{k=1}^{N} A_{ik} S_{ok} \quad \text{and} \quad \sum_{k=1}^{N} S_{ok} = 1, \tag{6.3}$$

where S_{ok} is a discrete, normalized $G\cos^{2s}$ shape, Eq. (6.1), and N is the number of directional bins; $\mathbf{A}^f$ is the linear transformation matrix for a fixed-shape incident spectrum and is formed from the original (larger dimension) matrix $\mathbf{A}$ of transformation coefficients for each directional bin (section 3). For fixed values of θ_p and s, the linearized problem (6.2) was solved for $\mathbf{E}_o$ using NNLS and a temporal smoothness constraint (since the observations are not hourly, but hourly S_o are sought). As in section 4, the observations were normalized by their statistical uncertainty. As in the previous linear inverse problem, a 36-h time period ($M = 36$) was considered, θ_p was varied in 5° increments between 160° and 335°. The spreading parameter s was assigned 12 values representing distributions with full widths at half maximum (FWHM) of 5°–60°. Thus, for a given frequency band, 432 linear inverse solutions (36 peak directions, each with 12 different directional widths) were obtained to map the entire solution space. The optimal values of θ_p, s, and $\mathbf{E}_o$ were those that resulted in the best overall fit to the observations (6.2) and temporal smoothness constraint. The number of unknowns was significantly reduced, and the dimensions of the kernel $\mathbf{A}$ are small compared to the more general problem (3c.2). Therefore, even though 432 separate linear problems are solved, finding the best values of $\mathbf{E}_o$, θ_p, and s required less than 5% of the CPU time needed to solve the previous problems. A temporal smoothness weight $w_t = 0.0005$ was chosen for the nonlinear inverse results presented (in Table 1 and Fig. 8) by examining the observation misfit. A wide range of w_t suppressed large, rapid temporal fluctuations in $\mathbf{E}_o$ without substantially degrading the fit to the observations.

For both the North and South Pacific swell events, the hindcast and inverse peak directions agree within the 5° resolution of the inverse method (Table 1). The inverse-estimated directional spread was also narrow, consistent with expectations for low-frequency, remotely generated southern swell (Munk et al. 1963). The observation misfits for the more highly constrained unimodal solutions (Fig. 8) were (as expected) larger than for the more general linear inverse results (Figs. 5 and 6), but still reasonably consistent with the expected statistical fluctuations in the observations.

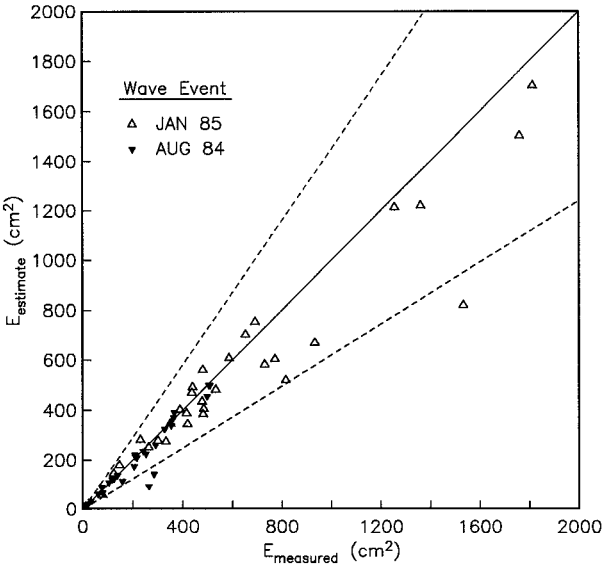

FIG. 8. Observation misfit of inverse-estimated energy for the two wave events with the a priori assumption of a $\cos^{2s}$ directional distribution (6.1) and temporal smoothness weight $w_t = 0.0005$.

The drastic assumption of a single directional peak with a $\cos^{2s}$ shape will be violated in many cases (Tyler et al. 1974; Regier and Davis 1977). Multiple deep ocean wave events in a single 0.01-Hz frequency band are common in southern California (Munk et al. 1963) and many other settings. A possible application of this highly constrained estimator is to qualitatively model extreme historical wave events where only a limited number of wave observations are available and the single dominant source assumption is reasonable. We used a 36-h time period to derive single, fixed values for θ_p and s. Shorter time periods must be used if these parameters are expected to vary significantly over 36 hours. Alternatively, the nonlinear inverse model could be generalized to include (smooth) temporal variations in s and θ_p, or entirely different parametric shapes could be used. The present results illustrate that the resolving power of the coastal observations can be significantly enhanced by invoking one of many plausible a priori assumptions about S_o.

7. Summary

Accurate, high-resolution estimates of offshore swell spectra S_o are needed to initialize numerical model predictions of the transformation of swell propagating over complex shelf bathymetry. Meteorological hindcasts alone are often inadequate for this purpose.

We utilize inverse methods to assimilate sheltered, coastal wave observations [(2.1) and (2.2)] into estimates of S_o. A spectral refraction model [(3a.2), Fig. 2] extended to include the time lags for wave energy to propagate between offshore and coastal measurement sites (3c.1) defines a linear relationship between S_o and coastal observations. This relationship is expressed as a linear set of equations with S_o discretized into a vector ($\mathbf{S}_o$) of frequency–direction–time components (3c.2).

In practice, the linear inverse problem is underdetermined; the unknown components of $\mathbf{S}_o$ greatly outnumbering coastal observations. Smoothness constraints in direction and time (4b.1) guarantee the existence of unique solutions. Whereas the relative importance of each observations can be weighed by its statistical uncertainty (4c.1), the weighting of directional and temporal smoothness is determined heuristically by examining the physical plausibility of $\mathbf{S}_o$ and the resulting observation misfit.

Historical wave data from the Southern California Bight (Fig. 1) are used to illustrate the inverse methods. In two examples, sheltered wave observations and smoothness constraints are used to constrain the estimates of S_o, and these estimates are compared to meteorological-based hindcasts of the offshore peak swell direction at the peak period. Good inverse–hindcast agreement was obtained for a January 1985 swell by solving (3c.2) using a linear inverse method (nonnegative least squares) with a range of smoothness weights and five coastal observation sites (Figs. 3 and 5). However, inverse–hindcast agreement for the peak direction was much poorer for a southern swell in August 1994 with four observation sites (Fig. 6a). Furthermore, for both swell events, the total (e.g., directionally integrated) offshore energy in the peak frequency band (Fig. 4) and the directional width of S_o were poorly resolved. Owing to a lack of completely unsheltered wave measurements and the limited number and locations of the coastal observations, a wide range of plausibly smooth offshore directional distributions are statistically consistent with the observations.

A nonlinear inverse method (6.1) using the a priori assumption of a $\cos^{2s}$ directional distribution accurately estimated the peak wave directions for both events, and the estimated narrow directional widths were consistent with distant generation (Table 1). However, a priori assumptions (e.g., a unimodal spectrum) should be supported by additional information (meteorological-based wave hindcasts in the present case). Even if the true spectrum is unimodal, deviations from a $\cos^{2s}$ shape will corrupt the inverse estimates in much the same way they degrade directional spectra estimates based on directional buoy data and an assumed $\cos^{2s}$ parametric form (Ochoa and Gonzalez 1990). Errors will be particularly large when there are multiple sources of comparably energetic swell at the same wave frequency. The tradeoff between smoothness, data misfits, and a priori assumptions in inverse estimates of the offshore frequency–directional spectra (from an incoherent array of sheltered sensors separated by many wavelengths) is quite similar to the tradeoffs encountered in estimating local frequency–directional spectra (from a coherent, spatially compact array spanning a few wavelengths or less, e.g., Davis and Regier 1977; Long and Hasslemann 1979; Herbers and Guza 1990).

Inverse estimator performance will vary according to the complexity of the geographic setting and wave field, and with the number and location of coastal observations. We conclude that, in the bathymetrically complex Southern California Bight, detailed estimates of the offshore directional distribution of remotely generated swell useful for regional swell prediction cannot be routinely inferred from the modest number of sheltered wave observations typically available. In Part II, the inverse method is generalized to use deep water hindcasts and unsheltered buoy measurements as primary constraints on S_o. Sheltered wave observations and linear wave theory are used to enhance the resolution and accuracy of these initial estimates. The inverse-estimated $\mathbf{S}_o$ are used to initialize the swell propagation model, thus combining offshore and sheltered wave information into regional swell predictions. A comprehensive dataset of offshore and sheltered wave measurements is used to validate the assimilation methodology.

Acknowledgments. This research was supported jointly by the California Department of Boating and Waterways (CDBW) wave data utilization program for furthering boating access and safety and the ONR Waves BAA and Coastal Sciences Programs. The wave data was collected by the Coastal Data Information Program (CDIP, supported by the Army Corps of Engineers and CDBW). Wave data acquisition was supervised by David Castel and Julie Thomas. Dr. Richard Seymour (CDIP principal investigator), and Dr. Reinhard Flick and Mr. David McGehee (CDIP program managers) encouraged and contributed significantly to the study. We are indebted to Steve Pawka, who first proposed applying inverse methods to the island sheltering problem in southern California. We thank Tom Herbers for his statistical wisdom and Nick Graham for providing the hindcasts.

APPENDIX

Observation Uncertainty

Each observation in the inverse problems in sections 4 and 6 was weighted inversely by its statistical uncertainty σ. With the assumption of many degrees of freedom (2ν), estimates of σ^2 for wave energy and the first four directional moments of a spectrum [$S(\theta)$, (2.2)] are (following Borgman et al. 1982)

$$\sigma^2\begin{bmatrix}\int d\theta\, S\\ \int d\theta\, S\cos\theta\\ \int d\theta\, S\sin\theta\\ \int d\theta\, S\cos 2\theta\\ \int d\theta\, S\sin 2\theta\end{bmatrix} = (E^2/\nu)\begin{bmatrix}1\\ 1/2(C+A^2)\\ 1/2(D+B^2)\\ C^2+D^2-2F^2\\ 2(CD+F^2)\end{bmatrix}, \quad \text{(A.1)}$$

where

$$E = \int d\theta\, S$$

$$A = \frac{1}{E}\int d\theta\, S\cos\theta$$

$$B = \frac{1}{E}\int d\theta\, S\sin\theta$$

$$C = \frac{1}{E}\int d\theta\, S\cos^2\theta$$

$$D = \frac{1}{E}\int d\theta\, S\sin^2\theta$$

$$F = \frac{1}{E}\int d\theta\, S\sin\theta\cos\theta. \quad \text{(A.2)}$$

REFERENCES

Borgman, L. E., R. L. Hagan, and T. Kuik, 1982: Statistical precision of directional spectrum estimation with data from a tilt-and-roll buoy. *Topics in Ocean Physics,* Societa Italiana di Fisica, 418–438.

Constable, S. C., R. L. Parker, and C. G. Constable, 1987: Occam's inversion: A practical algorithm for generating smooth models from electromagnetic sounding data. *Geophysics,* **52**(3), 289–300.

Davis, R. E., and L. A. Regier, 1977: Methods for estimating directional wave spectra from multi-element arrays. *J. Mar. Res.*, **35,** 453–477.

Dorrestein, R., 1960: Simplified method for determining refraction coefficients for sea waves. *J. Geophys. Res.,* **65**(2), 637–642.

Elgar, S., and R. Seymour, 1985: Effects of the lack of stationarity on deep water wave statistics, Conference Record, *Oceans '85, Ocean Engineering and the Environment,* San Diego, CA, Mar. Technol. Soc., 718–722.

Graber, H. C., M. W. Byman, and W. Rosenthal, 1990: Numerical simulations of surface wave refraction in the North Sea. Part 1: Kinematics. *Dtsch. Hydrogr. Z.,* **43,** 1–18.

——, ——, and H. Gunther, 1991: Numerical simulations of surface wave refraction in the North Sea.. Part 2: Dynamics. *Dtsch. Hydrogr. Z.,* **44,** 1–15.

Herbers, T. H. C., and R. T. Guza, 1989: Estimation of wave radiation stresses from slope array data. *J. Geophys. Res.,* **94**(C2), 2099–2104.

——, and ——, 1990: Estimation of directional wave spectra from multi-component observations. *J. Phys. Oceanogr.,* **20,** 1703–1724.

Higgins, A. L., R. J. Seymour, and S. S. Pawka, 1981: A compact representation of ocean wave directionality. *Appl. Ocean Res.,* **3,** 105–112.

Lawson C. L., and R. J. Hanson, 1974: *Solving Least Squares Problems.* Prentice-Hall, 340 pp.

LeMehaute B., and J. D. Wang, 1982: Wave spectrum changes on a sloped beach. *ASCE J. Waterway, Port, Coastal Ocean Eng.,* **108**(WW1), 33–47.

Long, R. B., and K. Hasselmann, 1979: A variational technique for extracting directional spectra from multi-component wave data. *J. Phys. Oceanogr.,* **9,** 373–381.

Longuet-Higgins, M. S., 1957: On the transformation of a continuous spectrum by refraction. *Proc. Cambridge Philos. Soc.,* **53**(1), 226–229.

——, D. E. Cartwright, and N. D. Smith, 1963: Observations of the directional spectrum of sea waves using the motions of a floating buoy. *Proc. Conf. Ocean Wave Spectra,* Prentice-Hall, 111–132.

Menke, W., 1984: *Geophysical Data Analysis: Discrete Inverse Theory.* Academic Press, 260 pp.

Munk W. H., G. R. Miller, F. E. Snodgrass, and N. F. Barber, 1963: Directional recording of swell from distant storms. *Philos. Trans. Roy. Soc. London A,* **255**(1062), 505–584.

Ochoa, J., and O. E. D. Gonzalez, 1990: Pitfalls in the estimation of wind wave directional spectra by variational principles. *Appl. Ocean Res.,* **12**(4), 180–187.

O'Reilly W. C., and R. T. Guza, 1991: Comparison of spectral refraction and refraction-diffraction wave models. *ASCE J. Waterway, Port, Coastal Ocean Eng.,* **117**(3), 199–215.

——, and ——, 1993: A comparison of two spectral wave models in the Southern California Bight. *Coastal Eng.,* **19**(3), 263–282.

——, R. J. Seymour, R. T. Guza, and D. Castel, 1994: Wave monitoring in the Southern California Bight, *Ocean Wave Measurement and Analysis: Proc. Second Int. Symp.,* New Orleans, LA, American Society of Civil Engineers, 849–863.

Pawka, S. S., 1983: Island shadows in wave directional spectra. *J. Geophys. Res.,* **88**(C4), 2579–2591.

Pierson W. J., J. J. Tuttle, and J. A. Wooley, 1953: The theory of the refraction of a short-crested gaussian sea surface with application to the northern New Jersey coast. *Proc. Third Conf. on Coastal Engineering,* American Society of Civil Engineers, 86–108.

Provost, C., and R. Salmon, 1986: A variational method for inverting hydrographic data. *J. Mar. Res.,* **44,** 1–34.

Regier, L. A., and R. E. Davis, 1977: Observations of the power and directional spectrum of ocean waves. *J. Mar. Res.,* **35**(3), 433–452.

Seymour, R. J., M. H. Sessions, and D. Castel, 1985: Automated remote recording and analysis of coastal data. *ASCE J. Waterway, Port, Coastal Ocean Eng.,* **111**(2), 388–400.

——, D. McGehee, D. Castel, J. Thomas, and W. O'Reilly, 1994: New technology in coastal wave monitoring, *Ocean Wave Measurement and Analysis, Proc. Second Int. Symp.,* New Orleans, LA, American Society of Civil Engineers, 105–123.

Tyler, G. L., C. C. Teague, R. H. Stewart, A. M. Peterson, W. H. Munk, and J. W. Joy, 1974: Wave directional spectra from synthetic aperture observations of radio scatter. *Deep-Sea Res.,* **21,** 989–1016.

U.S. Army Corps of Engineers, 1988: Historic wave and sea level data report: San Diego region. Ref. CCSTWS 88-6, U.S. Army Corps of Engineers, Los Angeles District, Planning Division, Coastal Resources Branch, 132 pp.

The WAMDI Group, 1988: The WAM Model—A third generation ocean wave prediction model. *J. Phys. Oceanogr.,* **18,** 1775–1810.